J. Materials, Conc. Struct. Pavements, JSCE, No. 760/V-63, 261-268, 2004 May

CRACKING MECHANISMS DUE TO CORROSION IN CONCRETE IDENTIFIED BY AE AND BEM

Farid UDDIN A.K.M.[1] and Masayasu OHTSU[2]

[1]Member of JSCE, PhD, Post-doctoral Fellow, Graduate School of Science and Technology, Kumamoto University (Kurokami 2-39-1, Kumamoto 860-8555, Japan)
[2]Member of JSCE, Dr. of Eng., Professor, Graduate School of Science and Technology, Kumamoto University (Kurokami 2-39-1, Kumamoto 860-8555, Japan)
ohtsu@gpo.kumamoto-u.ac.jp

Due to expansion of corrosive product, various patterns of cracks are nucleated around reinforcement in concrete. Crack kinematics are identified by acoustic emission (AE)-SiGMA (Simplified Green's function for Moment tensor Analysis) procedure. Numerical analysis is conducted by the boundary element method (BEM) based on the concept of the linear elastic fracture mechanics (LEFM). Crack traces due to corrosion are simulated by the two-domain BEM. The behaviors of the dimensionless stress intensity factors (K_I/K_{IC} and K_{II}/K_{IC}), and the cracking modes are studied for the different types of crack patterns. It is found that cracking mechanisms due to corrosion of reinforcement are mostly associated with the mode-I failure.

Key Words: *corrosion of reinforcement, crack initiation and propagation, boundary element method (BEM), acoustic emission (AE), stress intensity factors*

1. INTRODUCTION

One of serious deteriorations in concrete structures can be attributed to corrosion of reinforcement. For making decision on maintenance and repair in reinforcement concrete, identification of cracking mechanisms due to corrosion is significantly important. Expansion caused by corrosion product generates cracking, of which mechanisms are investigated analytically by boundary element method (BEM)[1].

The effect of cracks on structural integrity is closely dependent on the location and the orientation of cracks. For example, initiation of tensile cracks perpendicular to the reinforcement is not as critical as diagonal shear cracks. The classification of crack types and the determination of crack orientations can be kinematically conducted by acoustic emission (AE)[2),3)] in addition to the locations. To decide repair works and to prevent impending failure, quantitative techniques for identification of cracking mechanisms due to corrosion is in practical demand. In the case of chloride-induced corrosion[4)], it is reported that corrosion cracking can be detected by AE technique[5)]. In this paper, quantitative AE waveform analysis[3)] is applied to corrosion cracking. This analysis gives information on crack types and orientations. Analytically, two-domain BEM is applied to predict crack extension[6)]. These two results are discussed to identify the cracking mechanisms due to corrosion.

2. EXPERIMENTS

Concrete specimens of dimension 25cm x 25cm x 10cm were cured in water for 28days in the standard room (20°C) and tested at the age of 90days approximately. Concrete was made up of mixture as water (W): cement (C): sand (S): gravel (G) = 0.5:1.0:2.41:2.95 by weight as given in **Table 1**. Fresh and mechanical properties are summarized in **Tables 1** and **2**. Mechanical properties are obtained from cylindrical specimens of 10cm diameter and 20cm height at the age of 28days. Here, the tensile strength was obtained by the split test. P-wave velocity was applied to AE-SiGMA analysis. Young's modulus of elasticity, Poisson's ratio and critical stress intensity factor were employed in BEM analysis.

Cracks due to rebar corrosion in concrete are generated in the long process and very difficult to be examined in the short time in laboratory tests.

Table 1 Mixture proportion and properties of fresh concrete

Mixture	Weight per unit volume (kg/m^3)				Max. aggreg size (G_{max})
	Water (W)	Cement (C)	Sand (S)	Gravel (G)	
Concrete	172	344	830	1021	20mm

W/C	s/a	Air-entrained admixture	Slump	Air content
50%	48%	104cc	7.3cm	5.5%

Table 2 Mechanical properties of hardened concrete

Compressive strength (MPa)	Tensile strength (MPa)	Poisson's ratio	Young's modulus (GPa)	P-wave velocity (m/sec)
37.9	3.03	0.22	29.7	4,730

Thus, to simulate corrosion cracking in concrete, hydrostatic pressure was introduced by employing expansive agent. To simulate corrosion cracking, dolomite paste as an expansive agent was inserted into a circular cavity of 3cm diameter in the specimen. AE events were detected by six-channel AE system. AE sensors (PAC, UT1000) were attached to the concrete specimen by using silicone grease as shown in **Fig. 1**. AE waves were amplified by 50dB with a preamplifier (Pre-A), and waveforms and parameters of those waves exceeding the threshold level 50dB were recorded by LOCAN analyzer (PAC) and analyzed by TRA212-AE system (PAC). By employing SiGMA code[3], each AE source was classified into a tensile crack and a shear crack. Arrangement of AE sensors with AE system is shown in **Fig.1**.

From the previous study[1], typical crack patterns are identified around the reinforcement due to corrosion, which are reproduced by the expansive agent around the cavity as shown in **Figs.2** and **3**. One is the surface crack, which propagates vertically to the surface in the region of concrete cover and is marked as Sv. Others are the spalling crack marked as Sc, the vertical crack marked as V, and the diagonal crack marked as D. In experiments, the effect of cover thickness was also investigated. Two specimens A-1 and A-2 with cover thicknesses 3cm and 8cm were prepared.

In specimen A-1, the spalling crack (Sc), the surface crack (Sv) and the diagonal crack (D) are observed after about 18hours elapsed as shown in **Fig.2**.

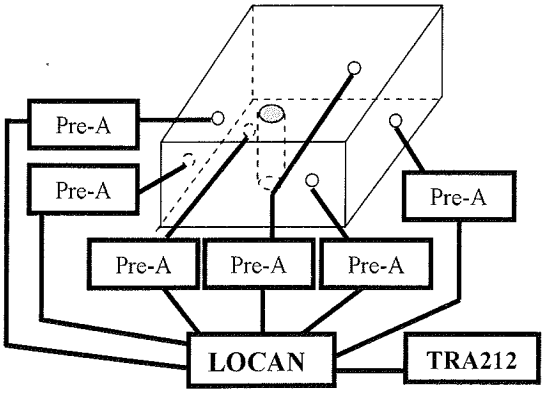

Fig.1 Arrangement of AE sensors and AE system.

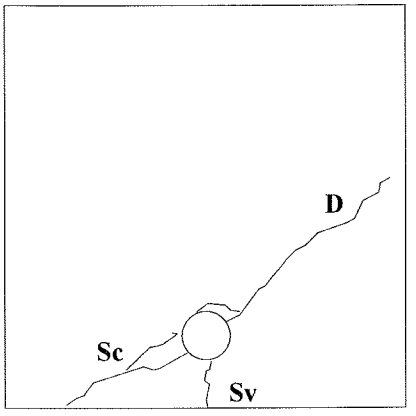

Fig.2 Observed cracks in specimen A-1 (3cm cover thickness).

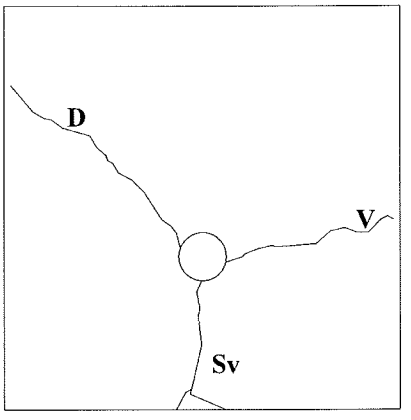

Fig.3 Observed cracks in specimen A-2 (8cm cover thickness).

In the case of cover thickness 8cm (specimen A-2), the surface crack (Sv), the diagonal crack (D), and the vertical crack (V) are observed as shown in **Fig.3**. The spalling crack could be nucleated in the case of the surface crack being arrested by aggregate[7]. Here, the vertical crack is observed in specimen A-2 instead of the spalling crack.

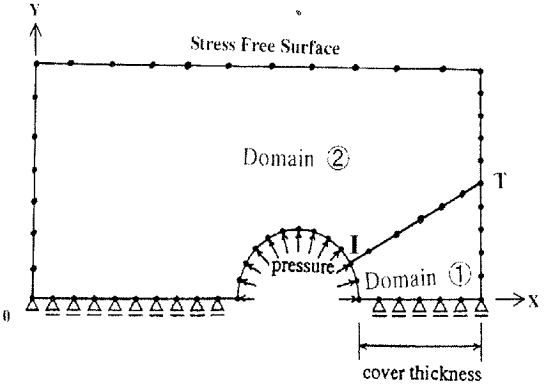

Fig.4 Two-domain BEM model for the spalling crack (Sc).

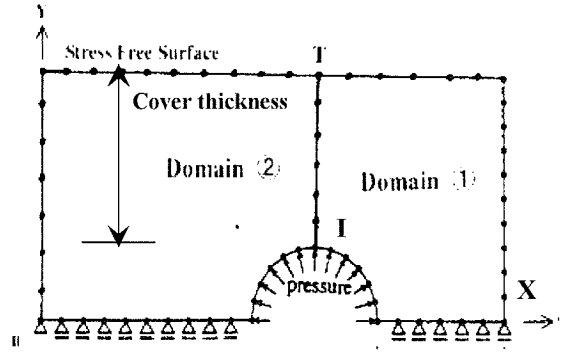

Fig.5 Two-domain BEM model for the vertical crack (V).

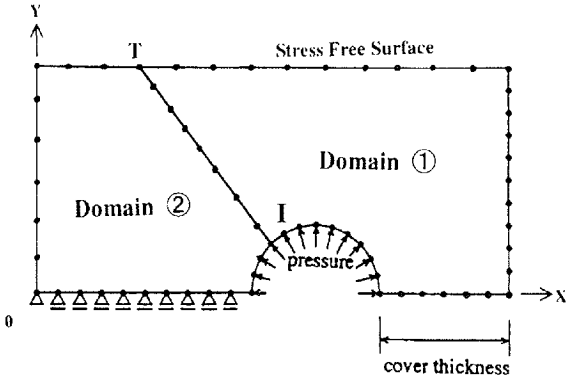

Fig.6 Two-domain BEM model for the diagonal crack (D).

3. ANALYTICAL MODEL

Models for the spalling crack, the surface crack, the vertical crack and the diagonal crack are analyzed by BEM. Some of analytical models are shown in **Figs. 4, 5** and **6**. They are similar to the models previously studied[1),7),8)]. Applying the two-domain BEM, the crack is initially modeled by a straight interface between domain 1 and 2. The interface is prescribed by the initial point (**I**), which corresponds to the starting point of the observed crack in the experiment, and the termination point (**T**), which is assumed as close as to the final crack trace. To identify cracking mechanisms of each crack trace, the observed cracks in **Figs. 2** and **3** are analyzed separately. This is because the order of crack nucleation is found in the previous study[1)]. The surface crack (Sv) is nucleated first, and then either the spalling crack (Sc) or the internal cracks of the diagonal (D) and the vertical crack (V) are generated. Thus, to analyze the latter three cracks, a half portion of the specimen is modeled as shown in **Figs. 4, 5** and **6**. As a result, the interaction with other cracks is neglected, as the central line of the specimen is replaced by the supporting boundary. In a similar manner, the surface crack is modeled as the same as **Fig. 5**. The effect of these models on the crack trace is known to be minor[1)], but the effect on pressure should be clarified and is under investigation.

The stress intensity factors K_I (mode I) and K_{II} (mode II) at the crack tip are determined from Smith's one-point formulae[9)]. K_I and K_{II} are determined from relative displacements at the crack tip elements. At each step of the analysis, the stress intensity factors are computed from the displacements of the crack-tip elements. When a crack propagates, the node at the crack tip is separated into two nodes and creating two stress-free elements in the direction θ. The stitching interface is created, connecting the crack tip with the termination point. Thus, a new crack is created automatically in an arbitrary direction. The direction of the maximum tangential stress θ is determined by the maximum circumferential stress by Erdogan-Sih criterion[10)] as,

$$K_I \sin\theta + K_{II}(3\cos\theta - 1) = 0 \tag{1}$$

$$\cos\frac{\theta}{2}\left[K_I \cos^2\left(\frac{\theta}{2}\right) - \frac{3}{2}K_{II}\sin\theta\right] = K_{IC} \tag{2}$$

From Eqs.(1) and (2), contribution K_I and K_{II} to K_{IC} can be obtained as the dimensionless stress intensity factors K_I/K_{IC} and K_{II}/K_{IC}[11)].

$$\left.\begin{aligned} K_I/K_{IC} &= \{(1-3\cos\theta)/\sin\theta\} / [\cos^3(\theta/2) \times \\ &\quad \{(1-3\cos\theta)/\sin\theta - {}^3/_2 \sin\theta/\cos^2(\theta/2)\}] \\ K_{II}/K_{IC} &= 1 / [\cos^3(\theta/2) \times \\ &\quad \{(1-3\cos\theta)/\sin\theta - {}^3/_2 \sin\theta/\cos^2(\theta/2)\}] \end{aligned}\right\} \tag{3}$$

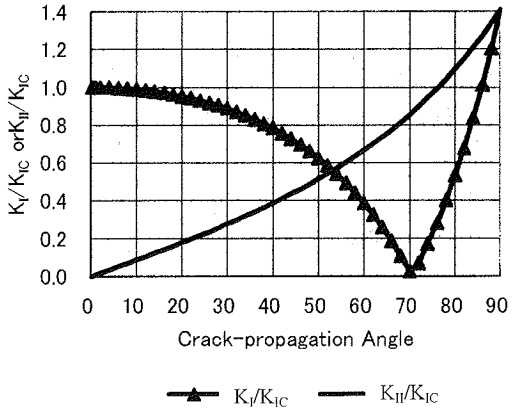

Fig.7 Characteristics curve for the dimensionless stress intensity factors with the variation of crack-propagation angle θ.

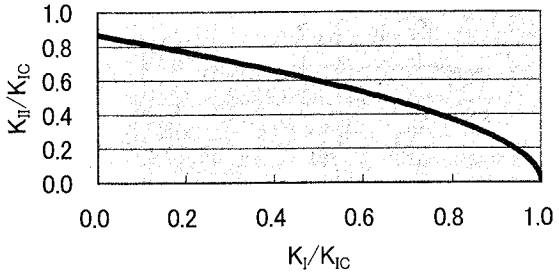

Fig.8 Characteristics curve for the relation between the dimensionless stress intensity factors.

where K_{IC} is the critical stress intensity factor and was determined in the previously studies[12]. By testing the same concrete mixture, it is found to be equal to 0.723MPa $m^{1/2}$.

The dimensionless stress intensity factors K_I/K_{IC} and K_{II}/K_{IC} with the variation of crack-propagation angle θ are plotted in **Fig.7**. These curves show that either mode I or mode II is dominant, depending on the crack-propagation angle θ. The mode I is dominant from $\theta=0^\circ$ to $\theta=53^\circ$ while mode II is dominant from $\theta=53^\circ$ to $\theta=90^\circ$. A relation between K_I/K_{IC} and K_{II}/K_{IC} is shown in **Fig.8**. Thus, the summation of K_I/K_{IC} and K_{II}/K_{IC} is not necessarily equal to 1.0 as obtained and discussed later.

All boundary meshes are of 5mm long but of 5.9mm long on the cavity as the projection angle is set to 22.5°. The effect of mesh sizes and the termination point on the numerical accuracy was previously studied[1),13)]. Based on these findings, the size of the mesh 5mm is selected in the present analysis. Because expansive agent was employed in the experiment, three types of expansive pressure are taken into consideration to simulate the expansion of corrosive products, which are uniform pressure, horizontal pressure and vertical pressure. Here, the horizontal is applied as just neglecting the vertical components of the uniform pressure. The vertical pressure is modeled as the other way.

4. IDENTIFIED MECHANISMS OF CRACK PROPAGATION DUE TO CORROSION

All AE sources analyzed by AE-SiGMA procedure are discussed in relation with the observed crack traces. These results are compared with those of BEM analysis. Thus, each crack observed is discussed one by one, as follows.

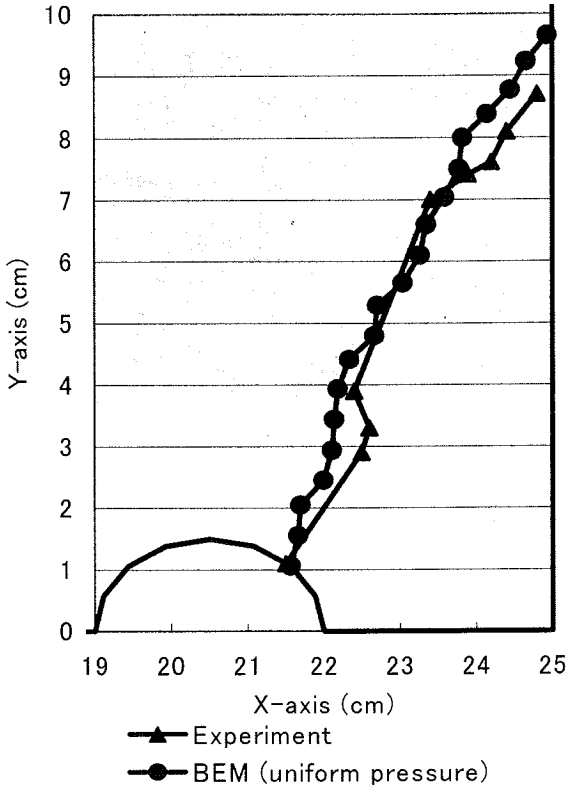

Fig.9 Traces of the spalling crack (Sc).

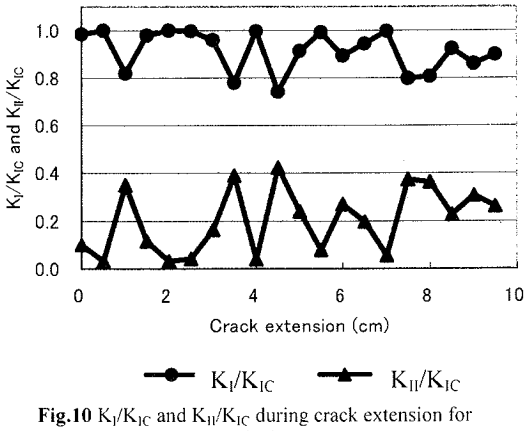

Fig.10 K_I/K_{IC} and K_{II}/K_{IC} during crack extension for the spalling crack (Sc).

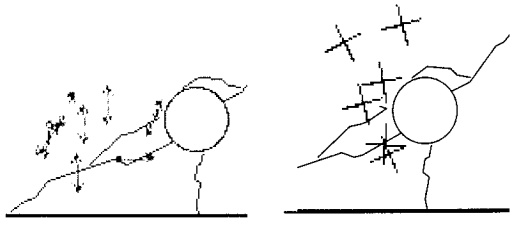

Fig.11 Locations of tensile cracks and shear cracks during crack extension for the spalling crack (Sc).

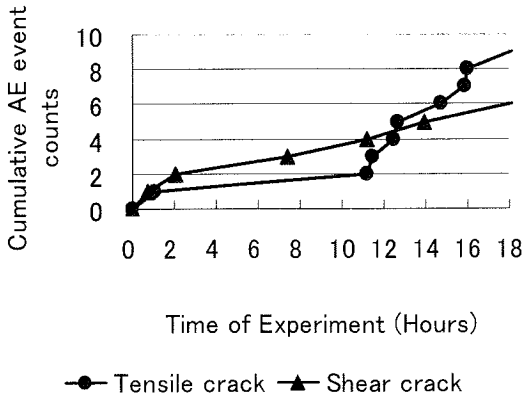

Fig.12 AE activities during crack extension for the spalling crack (Sc).

Spalling crack (Sc)

The spalling crack (Sc) in specimen A-1 is analyzed. Under hydrostatic pressure distribution, crack trace analyzed by BEM is plotted along with the actual crack trace in the experiment in **Fig.9**. Through cracking steps, reasonable agreement between the actual crack trace in the experiment and that of BEM analysis is observed. It is noted that crack trace due to the uniform pressure is the closest to the actual trace in the experiment out of any other pressure distributions. This is probably because the corrosion product is simulated by expansive agent.

The dimensionless stress intensity factors K_I/K_{IC} and K_{II}/K_{IC} are calculated at each step of crack extension by substituting crack-propagation angles into Eq.(3). Results are given in **Fig.10**.

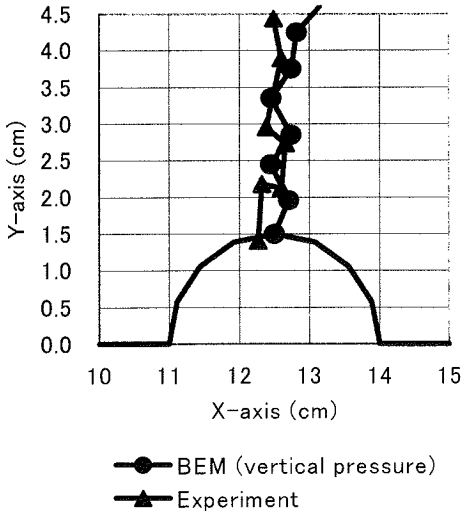

Fig.13 Traces of the surface crack (Sv).

The dimensionless stress intensity factors K_I/K_{IC} and K_{II}/K_{IC} are calculated at each step of crack extension by substituting crack-propagation angles into Eq.(3). Results are given in **Fig.10**. In the previous report[1], just the ratios of K_I to K_{II} are discussed without taking into account the crack angle θ. In the present paper, the angle is taking into consideration. Thus contribution of mode I (K_I/K_{IC}) and mode II (K_{II}/K_{IC}) are clearly discriminated. In the beginning of crack extension, K_I/K_{IC} is nearly equal to 1.0, so the pure mode I fracture occurs. Although K_{II}/K_{IC} increases gradually, tensile crack is always dominant.

According to AE-SiGMA analysis in **Fig.11**, both tensile and shear cracks are observed. For shear cracks, directions of a crack vector and a crack normal are indicated by the cross symbol (×) at their locations. Tensile cracks are located at their locations with the crack-opening direction by the arrow symbol (↔). It is observed that shear cracks are observed near the cavity. Tensile cracks are dominant, approaching the stress-free surface. Activity of these cracks is summarized in **Fig.12**.

As can be seen in **Fig.10**, at the middle stage of crack extension, contribution of K_{II} increases which may correspond to the increase of shear creak in **Fig.12**. In the middle of crack extension shear cracks are slightly active but then tensile cracks dominate again. From these results, it can be concluded that for propagation of the spalling crack (Sc), tensile cracks eventually dominate shear cracks.

Surface crack (Sv)

The surface crack (Sv) in specimen A-1 is analyzed with the stress free boundary condition at the cover concrete with half portion of the cavity

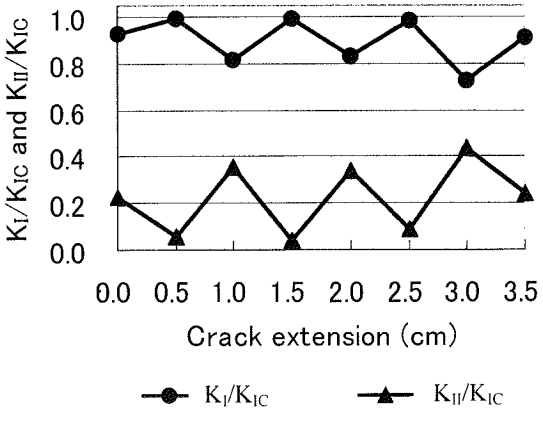

Fig.14 K_I/K_{IC} and K_{II}/K_{IC} during crack extension for the surface crack (Sv).

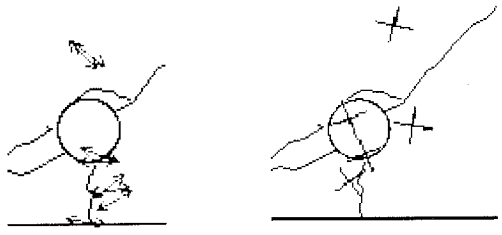

Fig.15 Locations of tensile cracks and shear cracks during crack extension for the surface crack (Sv).

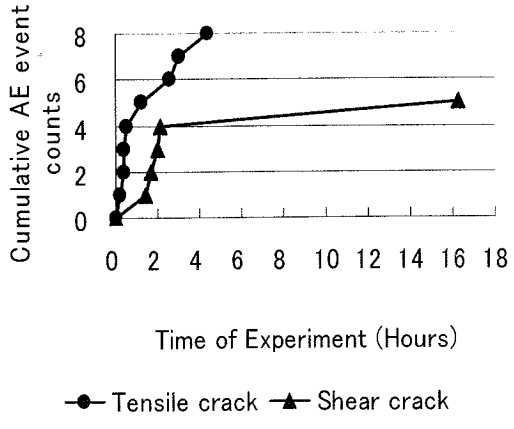

Fig.16 AE activities during crack extension for the surface crack (Sv).

under three kinds of pressure distributions simulating the crack. To model the crack as a similar model in **Fig.5**, it was assumed that the upper half portion over the cavity has little effect on the crack extension. Crack trace due to vertical pressure in BEM is plotted along with actual crack trace in the experiment in **Fig.13**. The analyzed crack trace is reasonably close to the actual trace in the experiment. This suggests that the pressure from the cavity mostly act vertically after the initiation of the crack.

The dimensionless stress intensity factors K_I/K_{IC} and K_{II}/K_{IC} are calculated at each step of crack extension. Results are given in **Fig.14**. In the beginning of crack extension, K_I/K_{IC} is nearly equal to 1.0. Although K_I/K_{IC} decreases and K_{II}/K_{IC} increases slightly, tensile crack is always dominant. The result of SiGMA analysis is given in **Fig.15**. Tensile cracks are observed close to the surface crack. From **Fig.16** on AE activity, it is observed that tensile cracks are dominant from the crack extension through the process. Similar results are observed in the surface crack in specimen A-2.

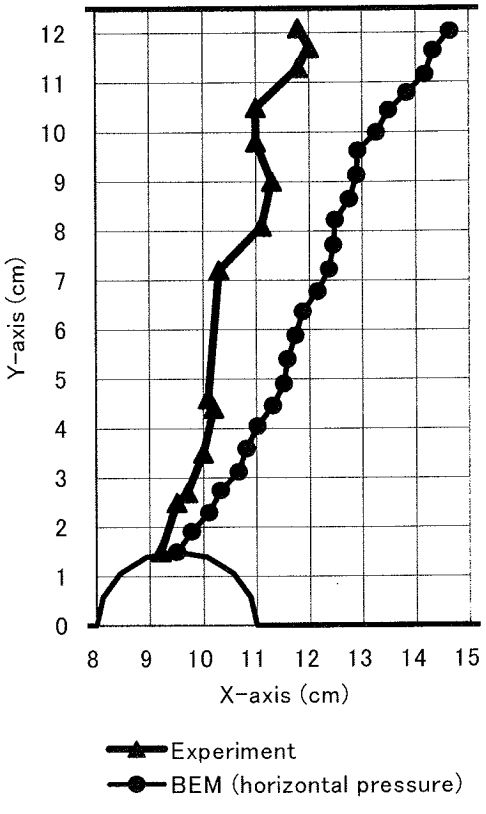

Fig.17 Traces of the vertical crack (V).

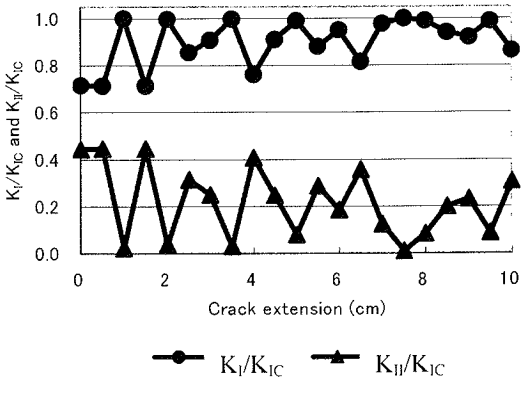

Fig.18 K_I/K_{IC} and K_{II}/K_{IC} during crack extension for the vertical crack (V).

Vertical crack (V)

The vertical crack (V) in specimen A-2 is analyzed with the stress free boundary condition at the cover thickness under three kinds of pressure distributions. Horizontal pressure distribution by BEM is plotted along with actual crack trace in **Fig.17**. This is because the crack trace due to horizontal pressure is the closest to the actual traces.

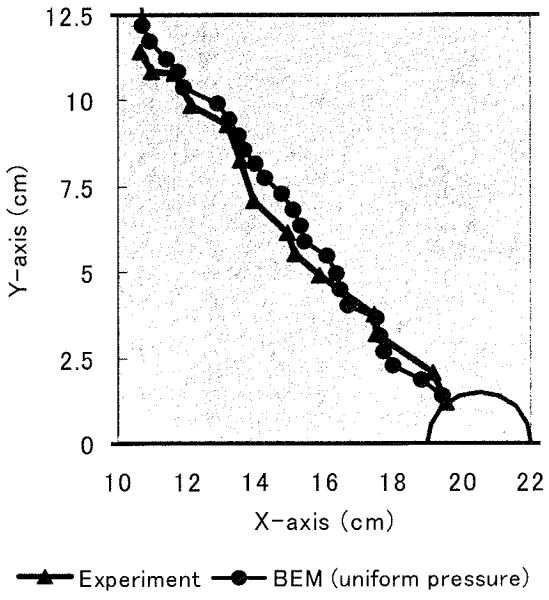

Fig.19 Traces of the diagonal crack (D).

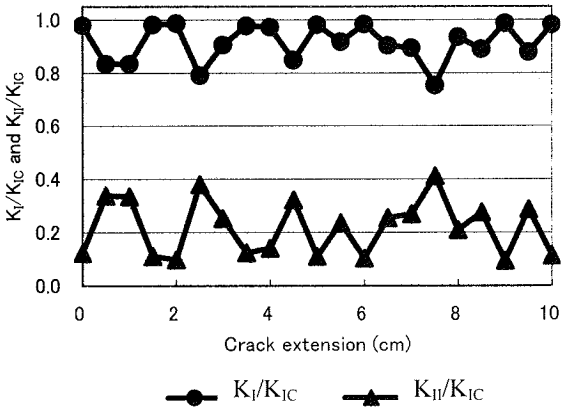

Fig.20 K_I/K_{IC} and K_{II}/K_{IC} during crack extension for the diagonal crack (D).

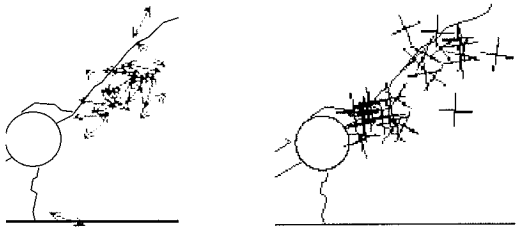

Fig.21 Locations of tensile cracks and shear cracks during crack extension for the diagonal crack (D).

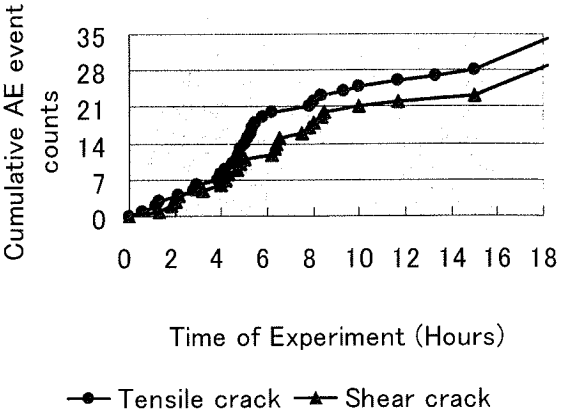

Fig.22 AE activities during crack extension for the diagonal crack (D).

The dimensionless stress intensity factors K_I/K_{IC} and K_{II}/K_{IC} are calculated at each step of crack extension. The results are given in **Fig.18**. During the crack extension, K_I/K_{IC} increases and K_{II}/K_{IC} decreases, although the mode II is quite active at the onset, compared with others. Because the number of AE events analyzed by SiGMA is few, no AE results are available for the vertical crack.

Diagonal crack (D)

The diagonal crack (D) in specimen A-1 is analyzed under three kinds of pressure distributions, simulating the crack extension after the surface crack. Crack trace due to uniform pressure in BEM is plotted along with actual crack trace in **Fig.19**. The analyzed crack trace is reasonably close to the actual trace in the experiment. This suggests that mechanisms of crack extension for the diagonal crack are associated with uniform pressure.

The dimensionless stress intensity factors K_I/K_{IC} and K_{II}/K_{IC} are calculated at each step of crack extension. Results are given in **Fig.20**. From the beginning of crack extension to the final, K_I/K_{IC} is nearly equal to 1.0, and so the mode I fracture is always dominant. Similar results are observed in the diagonal crack in specimen A-2.

According to SiGMA analysis in **Fig.21**, tensile cracks and shear cracks are observed close to the diagonal crack (D). From **Fig.22**, it is observed that tensile cracks are dominant to shear cracks. Thus, it is known that during extension of the diagonal crack, tensile cracks dominate shear cracks. Although the mechanism of the diagonal crack was concluded as mode II fracture in the previous study[1], the mode I is actually dominant in the diagonal crack by taking into account the angle of crack orientation in Eq.(3).

5. CONCLUSION

Crack propagation due to corrosion of reinforcement in concrete is studied analytically and experimentally. A two-domain BEM is applied to the mixed-mode crack extension based on the maximum circumferential stress criterion.

Traces of the spalling crack, the surface crack, the vertical crack and the diagonal crack in the arbitrary direction are analyzed. These cracks produced by employing expansive agent into concrete specimen. Cracking mechanisms are investigated by BEM and AE-SiGMA analysis. Depending on the crack types, contributions of mode I and mode II are varied during crack extension. Still, it is confirmed that cracking mechanisms due to simulated rebar corrosion in concrete is mode I fracture being dominant in all the type of cracks. Thus, the previous finding on the cracking mechanisms of the diagonal crack is updated[1].

ACKNOWLEDGEMENT: The authors wish to thank Assoc. Prof. M. Shigeishi, research technician Mr. Y. Tomoda and graduate student Mr. K. Ishiharaguchi in Kumamoto University for their substantial assistance in carrying out experiments and analyses.

REFERENCES

1) Farid Uddin, A.K.M. and Ohtsu, M.: BEM Analysis of Mixed-Mode Crack Propagation due to Corrosion of Reinforcement in Concrete. J. of Materials, Concrete Structures and Pavements. JSCE, No.704/V-55, pp.271-280, 2002.
2) Ohtsu, M.: Source Mechanism and Waveform Analysis of Acoustic Emission in Concrete. J. of AE, 2(1), pp.103-112, 1982.
3) Ohtsu, M.: Simplified Moment Tensor Analysis and Unified Decomposition of AE Source, J of Geophys. Res., 96, pp.6211-6221, 1991.
4) Hansson, C.M.: Concrete: The Advanced Industrial material of the 21st Century, Metallurgical and Materials Transactions. Vol.26A, No.6, pp.1321-1341, 1995.
5) Li, Z., Li, F., Zdunek, A., Landis, E., and Shah, S.P.: Application of Acoustic Emission Technique to Detection of Reinforcing Steel Corrosion in Concrete, ACI Materials Journal, Vol.95, No.1, pp.68-76, 1998.
6) Chahrour, A.H., Fukuchi, S., Ohtsu, M., and Tomoda, Y.: BEM Analysis of Mixed-Mode Crack Propagation in Center-Notched Concrete Beams. Transactions of JCI, Vol.15, pp.201-208, 1993.
7) Ohtsu, M. and Yoshimura, S.: Analysis of Crack Propagation and Crack Initiation due to Corrosion of Reinforcement. J. of Construction and Building Materials, Vol. 11, Nos. 7-8, pp.437-442, 1997.
8) Chahrour, A.H., and Ohtsu, M.: Multi-Domain BEM Implementation for Mixed-Mode Cracking in Concrete, Fracture and Damage of Concrete and Rock, FDCR-2, E & FN Spon, London, pp.196-205, 1992.
9) Smith, R.N.L. and Mason, J.C.: A Boundary Element Method for Curved Crack Problems in Two Dimensions, Boundary Element Methods in Engineering, Springer-Verlag, Berlin, pp.472-484, 1982.
10) Erdogan, F. and Sih, G.C.: On the Crack Extension in Plates under Plane Loading and Transverse Shear, J. of Basic Eng., No.12, pp.519-527, 1963.
11) Carpinterri, A.: Mechanical Damage and Crack Growth in Concrete, Martinus Nijhoff Publishers, Dordrecht, the Netherlands, 1986.
12) Farid Uddin, A.K.M. and Ohtsu, M.: Application of AE to Fracture Toughness and Crack Analysis by BEM in Concrete, the e-Journal of Nondestructive Testing – ISSN: 1435-4934, Issue Vol.7 No.9, 2002.
13) Chahrour, A.H., and Ohtsu, M.: Crack Growth Prediction in Scaled Down Model of Concrete Gravity Dam, Theoretical and Applied Fracture Mechanics, 21, pp.29-40, 1994.

(Received December 18, 2002)

AE法とBEM解析による腐食ひび割れの発生機構の解明

Farid UDDIN A.K.M.・大津政康

鉄筋コンクリート部材に発生する腐食ひび割れの発生機構の解明をAE法と境界要素法（BEM）解析によって行った．膨張材を用いた試験において，腐食ひび割れを観察し，AE-SiGMA解析を適用しクラックの機構同定を試みた．一方，BEM解析ではひび割れ軌跡を，2領域BEM法により解析し，軌跡の一致を確認した上で，ひび割れモードの同定を既報を参考に伝播方向を方向を考慮して実施した．その結果，表面ひび割れ，剥離ひび割れ，内部ひび割れに応じてモードIとモードIIの寄与率は異なるが，全般を通してひび割れ伝播過程は，モードIの開口モードが卓越することが明らかになった．